SCHOOL OF PHYSICS AND ASTRONOMY

YEAR 3 FINAL PROJECT REPORT

SESSION 2020-2021

Name:	Louie Leverett
Student Number:	C1823166
Degree Programme:	MPhys Physics with Astronomy
Project Title:	Hardwiring Supernovae information: model the spectral energy distribution
Supervisor:	Dr Cosimo Inserra
Assessor	Dr Paul Clark

Declaration:

I have read and understand Appendix 2 in the Student Handbook: "Some advice on the avoidance of plagiarism".

I hereby declare that the attached report is exclusively my own work, that no part of the work has previously been submitted for assessment (although do note that material in "Interim Report" may be re-used in the final "Project Report" as it is considered part of the same assessment), and that I have not knowingly allowed it to be copied by another person.

Analysing magnitude data of SN 2012fr to determine when spectral energy distributions of Type Ia supernovae are blackbodies

Cardiff University

School of Physics and Astronomy

By Louie Leverett

Academic supervisor: Dr Cosimo Inserra

Abstract

This report seeks to discuss and analyse fundamental properties of a SN 2012fr (a Type Ia SNe) by utilizing UV, optical and NIR photometry over the associated wavebands to produce SED's across 45 epochs in SN evolution. The focus of this research is to understand when it is appropriate to apply Planck's blackbody function as an approximation to the SN SED's and therefore decide if SN 2012fr is in fact a blackbody. It is found in this research that overall SN 2012fr does emit radiation as a blackbody particularly in the first 30 days of its evolution. However, chi-square (goodness) of fit plots highlight that this is not the case in later epochs, from around +40 days after maximum brightness of and beyond. It was noticed that the decrease in quality of the Planck approximation was due to the dramatic increase in the NIR contribution to the SN spectra and decrease in UV. Further analysis of Planck's approximation is discussed with the aid of the measurements for temperature, radius, and energy emission throughout SN 2012fr's evolution.

Abbreviation list

M – Mass

M_{solar} – Solar mass

M_B – B-magnitude

SN – Supernova

SNe – Supernovae

WD – White dwarf

Z – Redshift

ISM – Interstellar medium

SED – Spectral energy distribution

EM – Electromagnetic

SBb – Barred Spiral (Edwin Hubble's galaxy classification scheme)

Contents

1. Introduction

1.1 Supernovae

Supernovae are a highly luminous and violent events in which a star explodes resulting in the mass ejection of its outer envelope at high velocities, typically within the order of 10,000 km/s (Jha et al., 2019). Supernovae are the result of either the collapse of a massive star ($M > 8M_{solar}$) or a thermonuclear explosion of a white dwarf (Jha et al., 2019). Supernovae are so luminous they can outshine the very galaxies they reside in and in some cases can appear (if close enough) as a new star in the sky; hence the name 'nova'. SNe Type Ia are the most luminous of the standard SN types, their typical absolute B magnitudes being as large as $M_B = -19.5 \pm 0.1$ (Longair, 2011). In general, any progenitor of $M > 8M_{solar}$ will end as some variation of a supernovae, a dramatic end to the power houses of the universe.

As mentioned, supernovae come in variations and so are classified into two basic types with many more subclasses depending on their spectral features and differences in light-curves. The two basic types are conveniently named Type I and Type II, their key distinction being the absence and presence of hydrogen lines in their observed spectra, respectively. For example, SNe Type Ia have an absence of hydrogen features in their spectra due to being associated to objects that have lost these envelopes either because of strong mass-loss from their surface, or because they involve the explosion of white dwarfs which lost these envelopes after they were formed (Longair, 2011).

1.2 Type Ia supernovae

Low mass stars ($M < 8M_{solar}$) eventually die as they do not have temperatures sufficiently high enough to ignite further nuclear fusion reactions than carbon/oxygen. At this point they are no longer stable and expel their outer layers until they reach their next equilibrium stage, a white dwarf. White dwarfs resist gravity's pull with electron degenerate pressure, where electrons are squeezed until there is no more space between them, therefore, maintaining Pauli's exclusion principle (Pauli's exclusion principle does not allow two identical particles of spin-1/2 to occupy the same quantum state). However, if matter is accreted from a companion star such as a red giant or is acquired from the direct collision of another WD (Kushnir et al., 2013) the star will no longer be stable due to the ignition of a runaway nuclear process. These interactions will cause the temperature to rise until carbon and oxygen in the core fuse, igniting a wave of runaway nuclear burning which propagates through the core in seconds (Jha et al., 2019). The white dwarf is completely destroyed during the thermonuclear explosion expelling material into the cosmos with velocities as high as 10,000 km/s (Jha et al., 2019).

SNe Type Ia show an absence of the Balmer series of hydrogen in their optical spectra at maximum brightness (Longair, 2011) however, they do show a strong silicon feature (also at maximum brightness) seen in figure 1. The Balmer series is the movement of an electron from energy level n to the 2^{nd} energy level. The absence of the Balmer series and the presence of silicon in optical spectra are responsible for the Type Ia subclass classification.

1.3 The importance of studying Type Ia supernovae

Type Ia supernovae are arguably the most important SN type to study, however, the physics of the explosion mechanism even today is still not fully understood, due to the many explosion mechanism theories and the possibility of different progenitors (Hillebrandt and Niemeyer, 2000). One of the key reasons Type Ia SN are such an important phenomenon to study is due to the properties of their light curves. It is seen that the light curves of different Type Ia SN are incredibly similar, seen in figure 2. With the use of a luminosity-width relation these SN can be used as distance indicators, otherwise known as standard candles. Therefore, SNe Type Ia can be observed at redshifts greater than one ($z > 1$) (Longair, 2011). This method enables the absolute magnitudes of very distant supernovae to be determined; very useful in finding the resulting values of the cosmological parameters $\Omega_{\Lambda,}$ Ω_0, intern

providing evidence that the Universe is accelerating and is dominated by dark energy with a negative pressure equation of state; $w \approx -1$ (Longair, 2011).

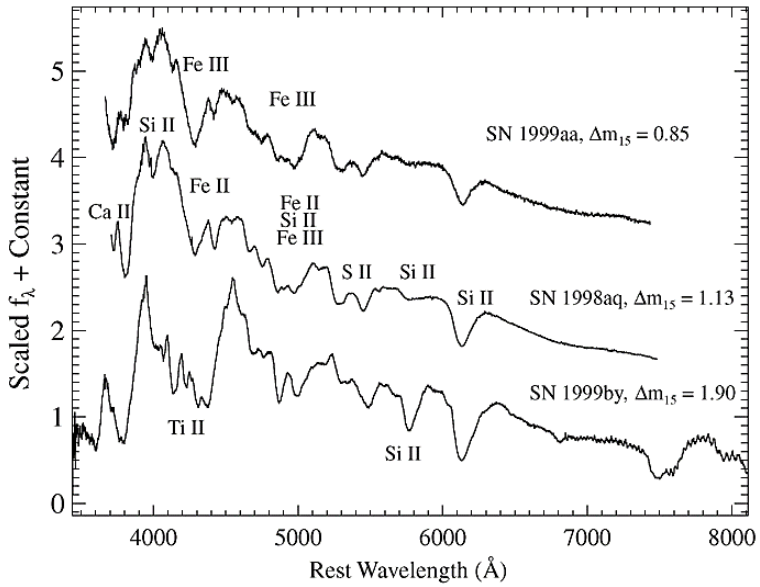

Figure 1 – Example spectra of Type Ia supernovae at B-band maximum, showing strong silicon features and the absence of hydrogen features (Matheson et al., 2008).

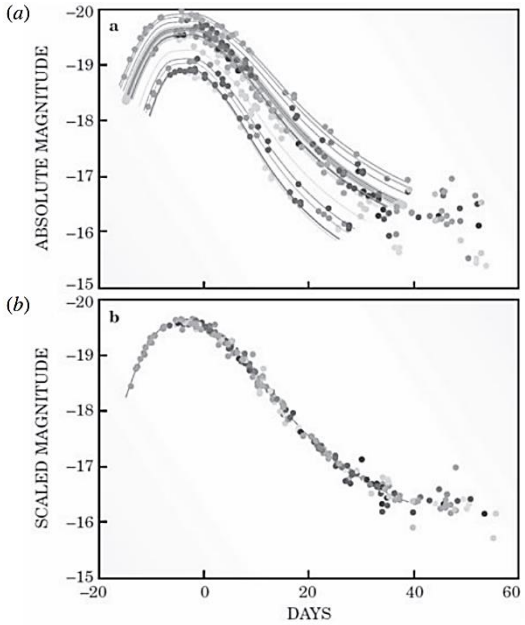

Figure 2 - (a) The light curves of a number of Type Ia supernovae, illustrating the luminosity–width relation. (b) Once account is taken of the luminosity–width relation, the light curves of Type Ia supernovae are remarkably similar and so can be used as distance indicators which can be observed to redshifts greater than one (Longair, 2011).

Not only are supernovae important in understanding the properties of the universe but they are also important to the galaxies they belong due to their role in the abundance and distribution of heavy elements in the ISM. The production of heavy elements during nucleosynthesis alone is an important feature of SNe.

The energy released during a SNe Type Ia ($\sim 10^{51}$ erg) (Jha et al., 2019) mainly comes from the difference in nuclear binding energy in the explosive fusion of light nuclei (mainly carbon and oxygen) into tightly bound nuclear "ash" dominated by iron and silicon group elements (group 8 on the periodic

table). The final outcome of the thermonuclear reactions is the formation of ^{56}Ni which undergoes electron-capture and β^+ decays to form ^{56}Co and then ^{56}Fe (Longair, 2011). It is this production of heavy elements and their various respective radioactive products that prolong light curves even after the initial explosion (Ellis, 2011). Most of the iron and manganese found in the sun and therefore, the solar system today was produced in a thermonuclear explosion of a white dwarf (Seitenzahl and Townsley, 2017). As a consequence of heavy element production, supernovae are vital in the distribution of metals (metals being any element heavier than hydrogen and helium produced in the Big Bang) among the ISM due to the vastness of supernovae.

1.4 Type Ia Supernovae evolution

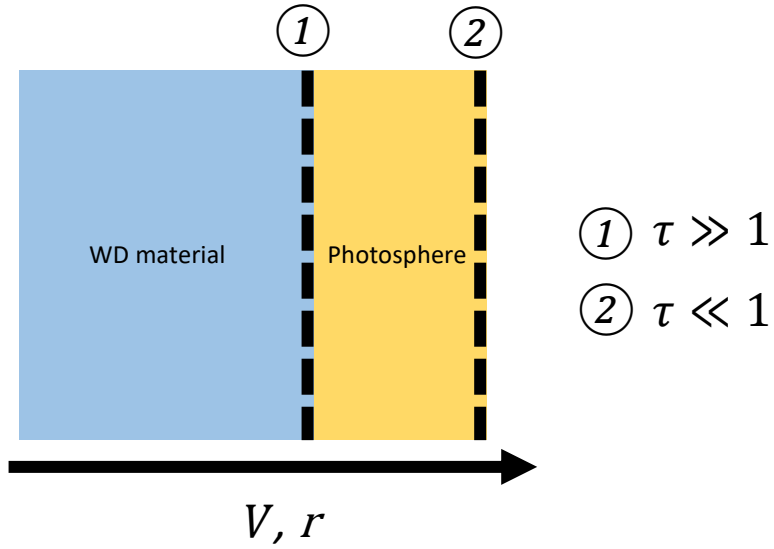

Figure 3 – Graphic showing expelled WD material after thermonuclear explosion showing the optically thick ($\tau \gg 1$) barrier and optically thin layer ($\tau \ll 1$) in the photosphere.

$$V \propto r \qquad \text{(Equation 1)}$$

To summarise section 1.2, a WD accretes material from either a companion main sequence star (single degenerate system) or from the collision with another white dwarf (double degenerate system). A runaway nuclear reaction then ignites the core of the carbon-oxygen white dwarf (Hillebrandt et al., 2013); known as deflagration and propagates rapidly outwards, converting carbon and oxygen to nickel through nucleosynthesis. Almost instantly the WD is completely annihilated in a thermonuclear explosion. The progenitor ejector are expelled at supersonic velocities (Pinto and Eastman, 2000) proportional to the radius at which the material started (equation 1).

The WD material is expelled as a photosphere, represented in figure 3. These mostly homogenous (Pinto and Eastman, 2000) bubbles of material is a distribution of optical thickness with increasing radius. The material goes from being completely opaque and therefore optically thick ① to being almost completely transparent and optically thin ②. Initially light curves are dominated by this optically thick region (τ>>1) in the photosphere as photons cannot escape the dense progenitor material without collisions or interaction. Lighter elements in the optically thin (τ<<1) envelope however do emit photons as it is a low-density medium allowing photons to be emitted with low chance of interaction. Due to its opacity the optically thick layer is considered a near perfect blackbody (see section 1.5) which has convenient qualities in which this research will be utilizing to determine properties of supernovae and its ejector.

During a SNe 99% of energy is released in the form of energetic neutrinos, the rest is converted into kinetic energy transferred into the progenitor's material. As the SN medium expands in radius with

time, its material collides with the surrounding ISM or previously ejected material during stellar mass loss.

1.5 What is a blackbody?

When a light ray passes through matter energy can be added or subtracted by emission or absorption of energy and so the intensity of light will likely not remain constant (Rybicki and Lightman, 2004). However, if the material that the light ray passes through is in thermodynamic equilibrium at temperature T, it will emit energy equal of that to what is absorbs, this matter in then known as a blackbody. When matter is in thermodynamic equilibrium, there is no net flow of thermal energy from the system, every absorption of a photon is compensated by the emission of another photon with the same energy (Ellis, 2011).

$$\frac{dI_\nu}{d\tau_\nu} = I_\nu - s_\nu \qquad \text{(Equation 2)}$$

If one considers the radiative transfer equation (see equation 2) where I_ν is the emission function and s_ν is the absorption function, then $\frac{dI_\nu}{d\tau_\nu} = 0$ when $I_\nu = S_\nu (= B_\nu)$ where B_ν is blackbody radiation described by the Planck function (see section 1.6). There are three important corollaries for blackbody radiation, $B_\nu(T)$:

i. Blackbody radiation is homogenous - radiation which has the same properties at every point without regularities
ii. Blackbody radiation is isotopic - the radiation emits uniformly in all directions
iii. Blackbody radiation, $B_\nu(T)$ is dependent on temperature T, not the shape or size of the container which holds the blackbody radiation

These corollaries are useful assumptions about supernovae and their evolution; seen presently.

1.6 Planck's function

$$B_\nu(T) = \frac{2h\nu^3/c^2}{\exp(h\nu/k_B T) - 1} \qquad \text{(Equation 3)}$$

$$B_\lambda(T) = \frac{2hc^2/\lambda^5}{\exp(hc/\lambda k_B T) - 1} \qquad \text{(Equation 4)}$$

The Planck function is the mathematical formulation of the blackbody emission spectrum in relation to frequency or equivalently wavelength and it describes the energy (ergs) emitted per unit time (seconds) per unit wavelength (Angstroms) per unit solid angle (steradian) from one square unit area (cm^2) of a perfect blackbody at temperature T; both varieties of the Planck formulation are seen in equations 3 & 4.

The derivation for Planck's function falls into two main parts, the derivation for the density of photon states in a blackbody and the average energy per photon state (Rybicki and Lightman, 2004). It is the average energy per photon which is responsible for the presence of the Planck constant since it is know from quantum physics that each photon of frequency ν has an energy $h\nu$. The origin of the Boltzmann constant comes from the probability of each photon state having an energy E_n since each state may contain n ($n = 0,1,2,3\ldots$) photons of energy $h\nu$ the energy then becomes $E_n = nh\nu$. Thus, according to statistical mechanics, the probability of a state of energy E_n is proportional to $\exp(-\beta E_n)$ where $\beta = (k_B T)^{-1}$ and k_B is the Boltzmann constant (Rybicki and Lightman, 2004). Planck's formulation of the blackbody unified the exponential increase in intensity of radiation formulated by Wien ($h\nu \gg k_B T$) and the gradually decreasing tail of Rayleigh-Jean's formulation ($h\nu \ll k_B T$). Both formulations could not explain the full blackbody spectrum, but this was no longer the case after Planck.

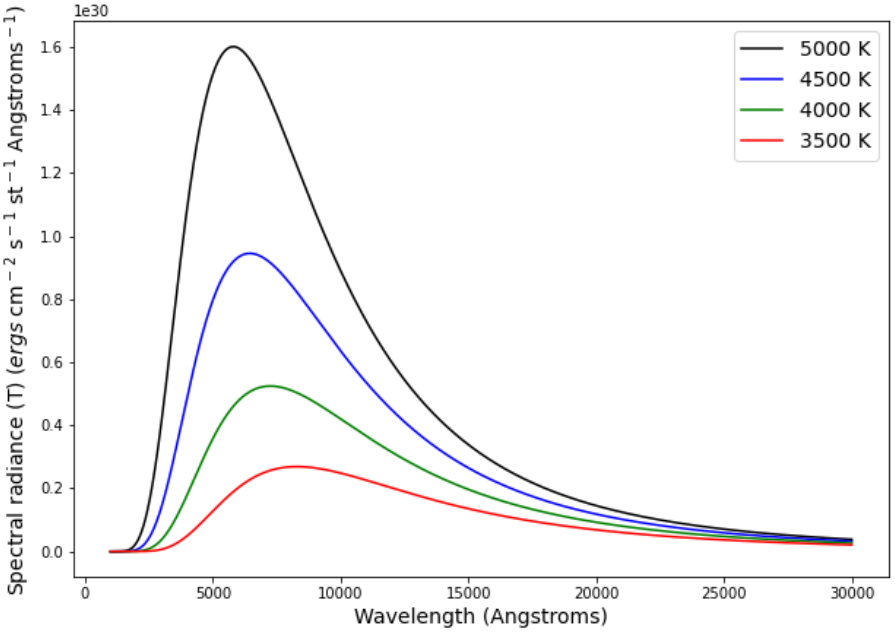

Figure 4 – A theoretical plot of Planck's function over a range of temperatures

The key property of Planck's mathematical formulation of blackbody radiation is its dependence on temperature of the blackbody and no other property. This can be seen in figure 4 where it is seen that the position of the peak depends on the temperature emitted by the object. In general, if the peak is higher and is shifted towards the shorter wavelengths this represents a higher temperature.

1.7 What is the purpose of this report?

This report seeks to discuss and analyse whether SED's of SN 2012fr plotted over a number of epochs resemble a blackbody spectrum. This approximation allows the fitting of Max Planck's mathematical formulation for a blackbody and therefore, measurements of temperature, radius, and energy to be made (see section 2). With the evolution of these properties with time and the quantification for the quality of Planck as an approximation to the SED's (see section 1.7.3), analysis can be performed to understand whether SN 2012fr is a blackbody, especially *when* this is the case. This report also includes light curves of SN 2012fr, seen in the appendix.

1.7.1 How is this project useful for understanding Type Ia SNe and their relation to Planck?

The explosion mechanism of SNe Type Ia is still largely debated (Hillebrandt and Niemeyer, 2000) since the progenitor star remains a mystery. Current research is unsure whether the cause of the thermonuclear explosion is due to WD accretion of a companion main-sequence star or the direct collision of another WD (Livio and Riess, 2003). Therefore, obtaining the fundamental properties (seen in this research project) of these mysterious events such as temperature, radius and energy and their evolutionary tracks with time may lead to evidence for either case of explosion mechanism.

Although this research may lead to the unravelling of the elusive progenitors, this is not the goal for of this research project. The goal of this research is to understand when it is appropriate to make the blackbody approximation to SED's of SN 2012fr and therefore make the same conjecture for all Type Ia supernovae. The approximation maybe more suitable at different times in the SN evolution and so may produce higher quality results with greater certainty depending on the time in its evolution.

1.7.2 What is a spectral energy distribution (SED)?

A spectral energy distribution is a plot of energy emitted by an object as a function of wavelength or frequency. An example of a SED can be seen in figure 4. Plotting such a distribution allows the

visualisation for the location for an objects peak EM emission over a broadband of wavelength or frequency.

1.7.3 What is chi-square?

The chi-square statistic is a non-parametric tool designed to analyse group differences when the dependent variable is measured at a nominal level (McHugh, 2013). In other words, the chi-square quantifies the "goodness" of fit and establishes how much a plotted distribution differs from a theoretical approximate distribution. In the context of this report the chi-square value represents how well the Planck function fits to the SED plots. A smaller chi-square value represents a closer fit to the data.

$$\chi^2 = \frac{(O-E)^2}{E} \qquad \text{(Equation 5)}$$

The general formula for the chi-squared goodness of fit can be seen in equation 5 where O is the observed values, E is the expected value and χ^2 is the Chi-squared value. A modified formulation of this equation is put into use in this research to compare Planck's function to SED's (see section 2.4).

1.8 Observations

This research focuses on SN 2012fr, a generic Type Ia SN found 3'' west and 52'' north from the centre of the SBb host galaxy NGC 1365, a member of the Fornax cluster. SN 2012fr was first discovered by the TAROT (*Télescopes à Action Rapide pour les Objets Transitoires*) collaboration at the La Silla Observatory, Chile on October 2012 UT with an open filter (i.e., no filter). Within a day and a half of discovery SN 2012fr was spectroscopically classified as a young, normal SN Ia which was caught well before maximum light. (Contreras et al., 2018)

1.8.1 Ultraviolet photometry

Ultraviolet imaging of SN 2012fr was performed from space with the swift UltraViolet Optical Telescope (UVOT); *Contreras 2018* (Contreras et al., 2018) only present uvw2, uvm2 and uvw1 passbands. A 3'' to 5'' source aperture was used for each image, depending on the signal to noise ratio.

1.8.2 Optical photometry

Optical imaging was obtained by the 1 metre Henrietta Swope telescoped located at LCO (Las Cumbres Observatory), equipped with Johnson (BV) and Sloan (ugri) filter set and a CCD detector. This is the main uBgVri – band photometry of SN 2012fr in the swope natural system tabulated in *Contreras 2018.* Optical photometry covers observations of ~180-day period starting the observations ~12 days before maximum light.

1.8.3 Confirmation and brightness images

La Silla-QUEST made observations of NGC 1365 a year before and found that the SN was not in any observations logged that year therefore proving that the SN had not been observed until October 2012.

Slooh space camera robotic telescope at Mt. Teide on the island of Tenerife made observations with a set of Astrodon Trubalance LRGB E-series filters less than two hours after the TAROT discovery image. These were important images as they provided information on brightness and colour of the SN shortly after the discovery of SN2012fr.

Confirming images of 2012fr were taken by Stu Parker at Parkdale observatory in New Zealand 1.3 days after discovery using a 0.36m Celestron telescope with SBIG ST-10XME CCD camera with no filter.

1.8.4 NIR photometry

NIR photometry was obtained by LCO du Pont 2.6 metre telescope with a RetroCam of a field of view: 3'.5 x 3'.5. Additional NIR imaging of SN 2012fr was obtained in J1, J and H filters using the FourStar camera attached to the 6.5 metre Magellan Baade telescope.

The magnitude data tabulated in (Contreras et al., 2018) covers observations over a large range of passbands from ~(3500 – 16500) angstroms.

1.8.5 Possible observational drawbacks

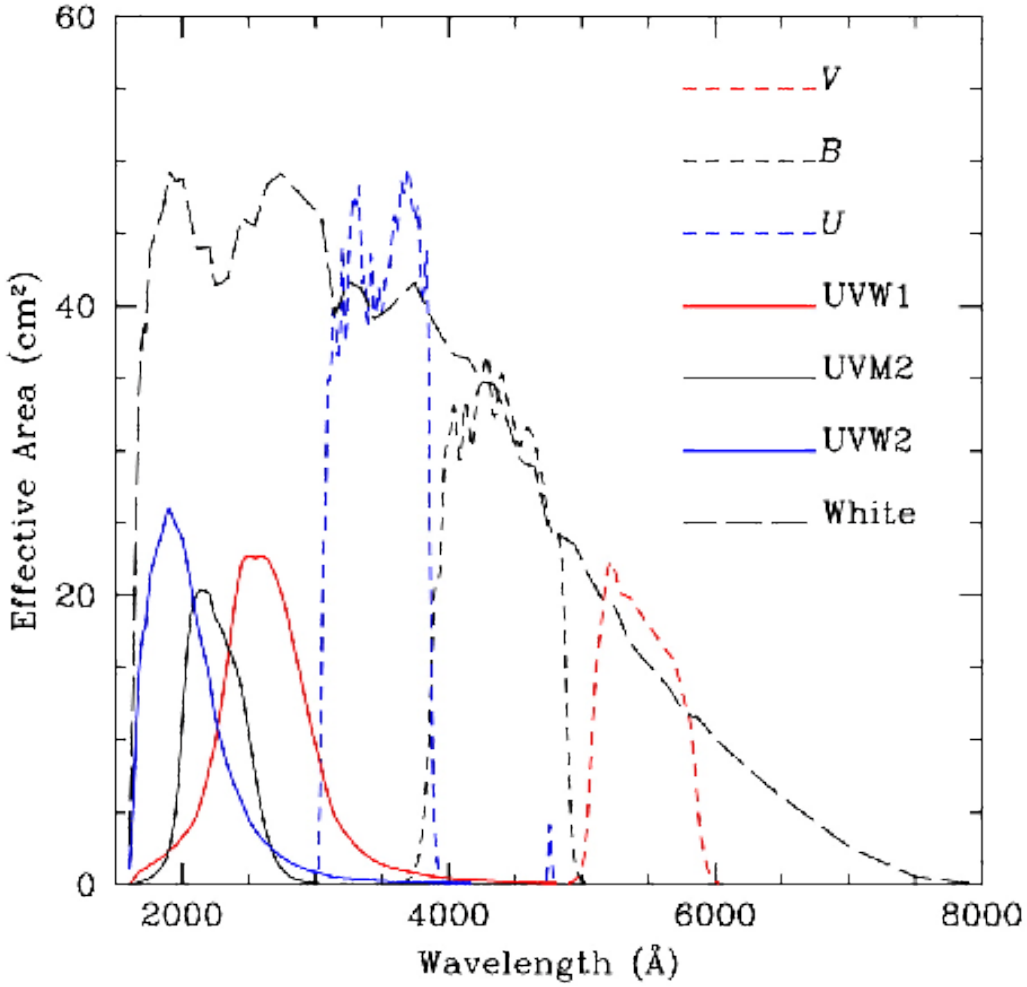

Figure 5 – Effective area curves for seven broadband UVOT filters shown as square centimetres versus wavelength in Angstroms.

Since all photometry observations were made by ground-based telescopes there may be some drawbacks to the observation quality. For example, the sensitivity in ultraviolet and low optical maybe be smaller than high optical or NIR passbands, this can be seen in figure 5 showing the effective area of UV filters with over wavelength compared to other high optical filters. The effective area is the area that must be used when calculating the physical properties of sources in the sky, e.g., surface brightness. Reflectivity and vignetting are just some of the effects that cause geometric area of a telescope to reduce the effective area. Figure 5 shows that ultraviolet filters (red, black, and blue solid lines) clearly have a smaller peak effective area, making them less sensitive than longer wavelength NIR filters seen in the red, black, and blue dashed lines.

Other effects that may cause greater noise in observations from ground-based telescopes. Firstly, the distortion of starlight from the atmosphere will cause a reduced quality in data collection. Although, the telescopes quoted in this report are high-altitude observatories reducing the effects of the atmosphere.

Secondly Moonlight may lighten the dark skies depending on the phase increasing the skyglow and further reducing quality of the data. However, a 50%-illuminated Moon has little effect unless it is close to the object being observed (Flanders, 2006).

2. Method

In this project UV, optical, and NIR broadband photometry has been used to calculate luminosity data for SN 2012fr with their respective wavelengths in order to plot SED's (spectral energy diagrams) covering many epochs of the SN evolution. Software was constructed to make fits of Planck's blackbody formula as an approximation to the data to assess how well the distributions resemble blackbody emission. If the assessment shows an overall successful fit (measured by the chi-square) an estimation for the temperature, radius and energy evolution can be made for the supernova. Measurements of photometry were made from UV through to NIR by different telescopes stated in section 1.8 and measurements are tabulated in (Contreras et al., 2018). The observational data was recorded as magnitude values for each filter (uBgVriYJH) from 12 days before maximum B brightness to 170 days after. Software for this research is developed in Python 3.8.8 making use of the Anaconda3 environment; all calculations and plots quoted in this research report were assembled in this software.

2.1 Plotting Spectral Energy Diagrams

$$F = F_0 \times 10^{\frac{m}{-2.5}} \quad \text{(Equation 6)}$$

$$D = 10^{(1+\frac{\mu}{5})} \quad \text{(Equation 7)}$$

$$L = 4\pi D^2 F \quad \text{(Equation 8)}$$

The magnitude data is converted into flux and then to luminosity using equations 6 & 8, respectively. F_0 in equation 6 is the flux zero-point values and are provided by (Bessell et al., n.d.) (also seen in the appendix of this report) and are used to calibrate a system to the standard magnitude system. The distance variable quoted in equation 7 makes use of the distance modulus recorded in (Contreras et al., 2018) to the host galaxy of the SN, NGC 1365 with a value of $\mu_B = 13.14 \pm 0.15\, mag$ with equation 7.

$$\sigma_{Flux} = \frac{|\sigma_{mag}| \times F}{1.09} \quad \text{(Equation 9)}$$

The propagation of error for transforming magnitude error to flux error was derived from the propagation of error equation and can be seen in equation 9. The derivation for equation 9 can be seen in the appendix. The error propagation in the luminosity calculations directly quote the flux error. Therefore, uncertainty values in flux and luminosity are calculated by inserting the uncertainty in the values before them into their respective equations. Consequently, the software is then left with luminosity values with uncertainties for across the filters of *uBgVriYJH* across all epochs. These data points are plotted against their respective central wavelengths in Angstroms. The central wavelengths are the weighted average of the spectral response weighted factor and are supplied by (Contreras et al., 2018) and are tabulated in the appendix. The central wavelengths cover a broadband of 3500-16000 Å. This method provides the software with the first SED and is the foundation for all other SED's plotted.

Since optical photometry was observed with a different telescope than NIR photometry the times at which the magnitude measurements are recorded for SN 2012fr between both observations are not adjusted to match the same epoch. Epochs were then decided by having measurements within a day of each other, this meant that not all the data could be used as not all the days had measurements for all filters. A simple script was programmed to iterate through both optical and NIR data tables to find matching epochs within a day of observations. This produced 45 epochs from the total 180 days of observation.

2.2 Fitting Planck's function

The mathematical formulation for Max Planck's blackbody distribution can be seen in equation 3&4 of section 1.6. Since one of the objectives of this research was to study the radius evolution in the software Planck's function is modified by multiplying it by the surface area of the SN photosphere, $4\pi R^2$ where R is the radius of the photosphere. All constants for Planck's function i.e., Boltzmann, Planck and the speed of light are quoted in the CGS (centimetre-gram-second) system of units since central wavelengths are too quoted in Angstroms in the SED plots.

```
popt, pcov = curve_fit(Planck, central_wavelength, L, p0 =
[Temperature, radius])

x_plot = np.linspace(1500, max(central_wavelength), num=1000)

yfit = Planck(x_plot, *popt)
```

Figure 6 – Curve_fit fitting function be called with fitting parameters. The preparation for its plot can be seen in the next two lines. 'yfit' is defined as the Planck function against x_plot with temperature and radius parameters guessed by Curve_fit.

As stated, the aim of this research is to determine whether Type Ia SNe are blackbodies by approximating Planck's function to SED's. Therefore, the software developed uses a non-linear least square fitting method to match a Planck function of temperature, T to the SED data set. The fitting method is a pre-programmed function provided by an external Python module: SciPy (version 1.6.3). This function takes various parameters utilised in this software, wavelength - the independent variable where the data is measured, luminosity – the dependent data, the initial guess for the parameters i.e., temperature and radius, and finally the guess function, Planck. The guess parameters used in the software for radius and temperature are 1e+15 cm and 10,000 K, respectively. The guess value for radius is a typical peak photosphere radius for a SN. The guess value for temperature is also typical of a SN photosphere. The fitting method uses these parameters to produce its own values for the guess parameters which can be applied to the Planck function in order to closely match the spectral energy distribution across the waveband. The outcome of a Planck approximation to an SED can be seen in figure 8 of section 3.1 with an epoch of 1.55 days.

2.3 Fitting 'weighted' Planck function

Another useful parameter input which the fitting method takes is 'sigma', this considers the standard deviations of errors in the 'ydata' (luminosity). The function takes an M-length sequence of uncertainties corresponding to the associated luminosity data. By default, this sequence is a series of ones. This application of the sigma allows a weighted fit of Planck to be plotted where the plot gives greater weight to the data points with smaller uncertainties and therefore should theoretically provide a higher quality fit since is accounts for data points with large uncertainties. The outcome of this first weighted plot for an epoch of 1.55 days is seen in section 3.1.

2.3.1 Ghost data

Since the outcome of the weighted fit was not desired (discussed in section 3.1) the plot required the addition of a UV ghost point to help provide a greater contribution of data to the shorter wavelengths and therefore produce something that resembled a Planck function. Therefore, a ghost point was chosen of a magnitude similar to the next data point along the broadband and with uncertainties evaluated as the average of all other data point uncertainties at that epoch.

Ghost points were added to epochs which did not present Planck distributions with the addition of sigma. It was found that many epochs across the evolution required a UV ghost point in order to produce expected measurements.

It was found after plotting a number of SED's that after the early time period of SN evolution the quality of the Planck fit and measurements reduced significantly, therefore, some quantitative assessment of how well Planck fitted the SED's was required to easily assess a reasonable fit.

2.4 Assessing chi-square

```
def chisq(popt, pcov):
    res = popt*-1
    perr = np.sqrt(np.diag(pcov))
    chisq = sum((res/perr)**2)
    return chisq
```

Figure 7 – Optimised chi-square function for evaluating the "goodness" of fit. Since pcov is a 2x2 matrix the errors for the values produced in popt are the diagonal of the matrix.

The chi-square is a method for measuring the "goodness" the fit is to the data. In the context of this research: how well does Planck fit to the SED data? Since the sigma provided to the fitting method is 1D and contains standard deviations of errors in the ydata, the optimised function is as follows in figure 7. A smaller chi-square value represents a closer fit of Planck to the SED data. The chi-square function in figure 7 takes the guess parameters produced by the fitting method and their errors.

2.5 Temperature evolution

As discussed in section 2 the temperature is estimated from the fitting method of the Planck function. To plot the evolution of this temperature with time, the temperatures were recorded over 45 epochs of fits providing 45 temperature data points over a time period of 180 days. The temperature (kelvin, K) was then plotted against time (days).

2.6 Radius evolution

Two methods were utilized to obtain the radius evolution of SN 2012fr's photosphere and are discussed presently.

2.6.1 Curve_fit method for approximating radius

As mentioned in section 2.2 the Planck function is modified by multiplying its intensity by the surface area of the photosphere, $4\pi R^2$. This provides the fitting method a second approximation it has to make based on a provided guess of the radius. The fitting method then produces the best approximation for the radius at the given epoch.

2.6.2 Stefan-Boltzmann method for approximating radius

$$P = A\varepsilon\sigma T^4 \qquad \text{(Equation 10)}$$

$$R = \sqrt[2]{L/4\pi\sigma T^4} \qquad \text{(Equation 11)}$$

This method utilizes the Stefan-Boltzmann equation (equation 10) and re-arranges the radius as the subject of the formula, seen in equation 11. The total power emitted by the SN is equivalent to the luminosity and is approximated by taking an integration of the Planck function at a given epoch. This combined with the measured temperature produces a measurement to the radius.

2.7 Energy emission

$$E = \pi \int_0^\infty B_\nu \, d\nu = \sigma T^4 \qquad \text{(Equation 12)}$$

Planck is a continuous function and therefore requires advanced calculus techniques to evaluate the integral of the function. The integral of the Planck function turns out to be the Stefan-Boltzmann Law which describes the total amount of energy given off by a blackbody each second (see equation 12). In this research however, the Planck function is multiplied by the surface area of the photosphere ($4\pi R^2$ where R is the radius of the photosphere) this means when the fitted Planck function is integrated it is measured to be the total energy emitted per second per area of the blackbody.

In order to integrate the Planck function, the software utilizes two integration methods: Simpson's rule and the Trapezium rule. These are pre-programmed functions imported from the SciPy module. Both methods were used to get a range of measurements as both methods have their advantages and disadvantages. The energies measured by these integration methods are then plotted with time to show the energy emitted by the SN over the observed evolution.

2.8 Light curves

Light curves are a plot of luminosity or magnitude evolution with time. The luminosity or magnitude of each filter is plotted with time showing the evolution for the intensity of emission from a particular wavelength. This highlights how each wavelength of light contributes to the SN evolution. These plots can be seen in figures 21 & 22 in the appendix of this report.

3. Results & discussion

In this section, calculated luminosity data from observations of SN 2012fr with telescope filters of u, B, g, V, r, I, J, H are plotted against their respective central wavelengths as a spectral energy distribution across the associated waveband. Planck's mathematical formulation of the blackbody distribution (see section 1.6) is fitted using the methods discussed in section 2 including a fit in consideration of uncertainties in the data. The uncertainties or 'statistical weight' is given to the data to assign a lighter, or heavier importance to data points with smaller or bigger uncertainties. The consideration of statistical weight will help compensate for data points with larger uncertainties and will (in theory) produce a higher quality fit.

This section also presents the evolution of temperature, radius, and energy with time. These plots are used to assess the quality of the Planck approximation to the SED's as they highlight clearly when the measurements made from Planck no longer fit to the expected relation.

3.1 Outcome of Spectral energy distribution plots

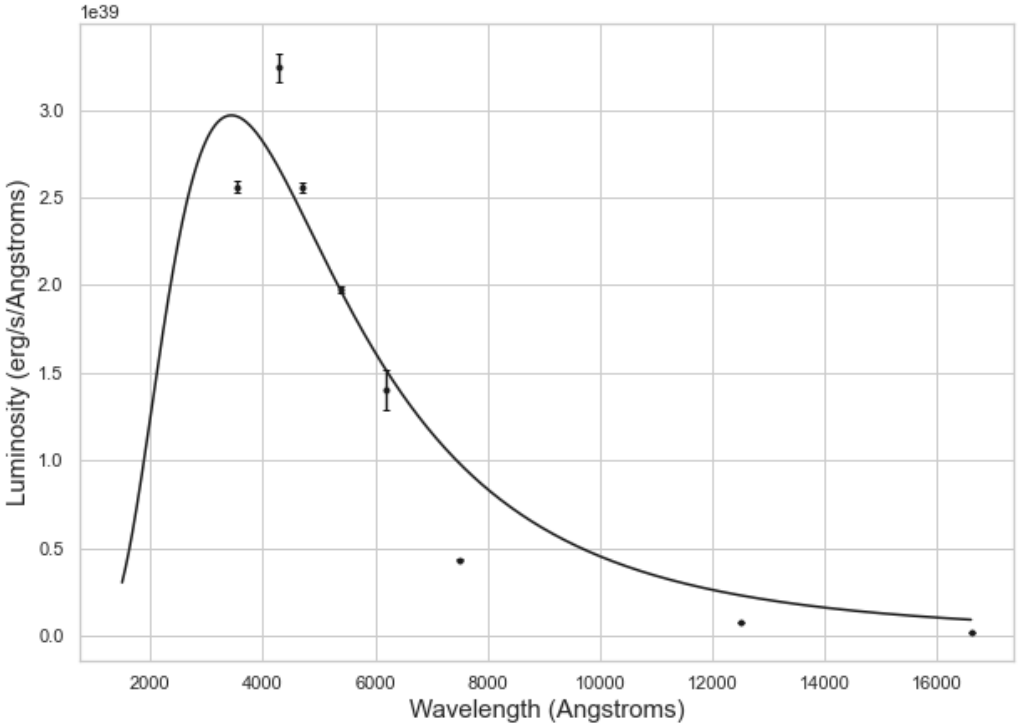

Figure 8 – Spectral energy distribution presenting luminosity data with error bars of 1σ*-uncertainty (circular points) against wavelength in Angstroms of SN2012fr at the epoch 1.55 days after maximum B-filter brightness. Planck's blackbody function is fitted to these data points (black solid line). Some error bars may be too small to be seen.*

Figure 8 shows a Planck approximation to a SED plotted at an epoch of 1.55 days after maximum B-filter brightness over a waveband of 1500 – 16600 Å. Planck's function is approximated to luminosty data points with a temperature and radius estimated by the fitting method discussed in section 2.2. Overall Planck fits the same general trend as the data and so shows good indication that the SED resembles a blackbody. The measurements of temperature, radius and chi-square from this Planck fit can be seen in table 1.

The shorter wavelength data points present greater uncertainties than the longer wavelength data points seen in their error bars in figure 8. This may be explained by the smaller sensitivity of observations seen in the UV (discussed in section 1.8.5 & 3.6). The error bars for the longer wavelength data points are encompassed by the data points themselves due to being so small.

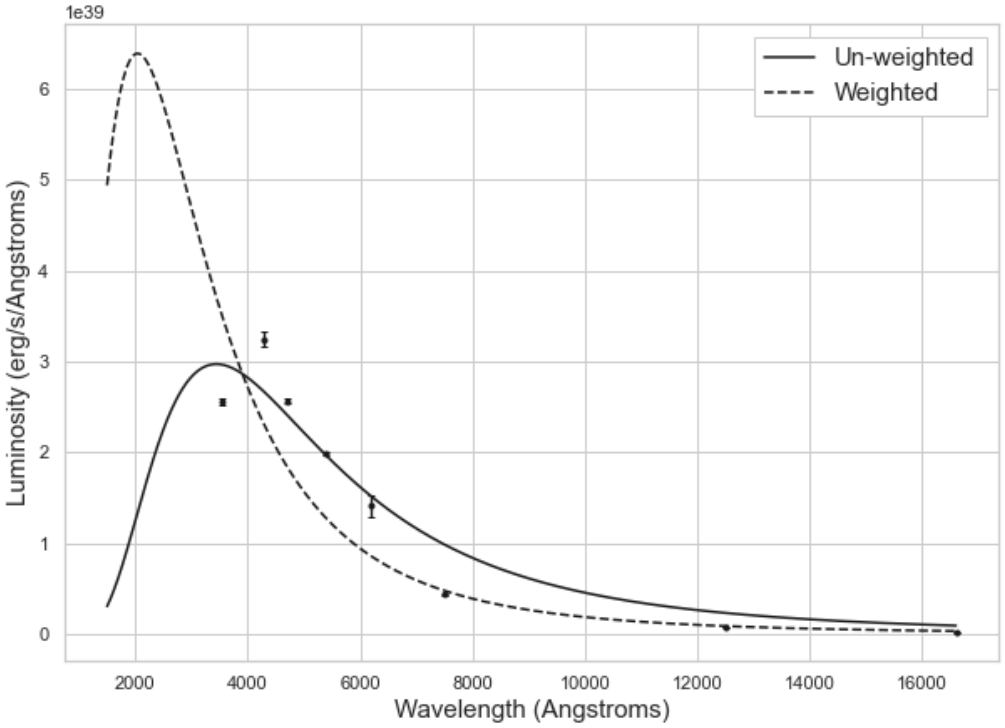

Figure 9 – Spectral energy distribution presenting luminosity data with error bars of 1σ*-uncertainty (circular points) against wavelength in Angstroms of SN2012fr at the epoch 1.55 days after maximum B-filter brightness. Planck's blackbody function is fitted to these data points (black solid line) with the consideration of statistical weight. Some error bars may be too small to be seen.*

$$\lambda_{max} = \frac{b}{T} \qquad \text{(Equation 13)}$$

As mentioned it is important to analyse the plot of Planck's function with the consideration of the uncertainties in the data. This plot is seen in figure 9 where the dashed black line is the 'weighted' approximation. This approximation does not resemble a Planck function as closley as the first Planck fit with no consieration of sigma. This maybe due to the decrease in the contribution of the UV (shorter wavelength) data points. If the weight of the UV data point is less than that of the longer wavelengths (NIR) then the peak of Planck's function will be higher, therefore measuring a higher temperature as shown with Wiens law (equation 13) where b is a constant of proportonality. Therefore, it may be sensible to assume that the Planck function may produce a higher quality fit with a greater sample of points in the UV.

Since there are no further UV measurements at this epoch the addition of a UV ghost point is employed to add greater weight to the UV end of the SED waveband. This is achieved in figure 10 with the addition of a ghost point at 3000 Å. Here, in comparison to figure 9 the peak has been pulled down making for a far more sensible approximation to a blackbody distribution. The difference in the measurements between the addition of a ghost point and not can be seen in table 1.

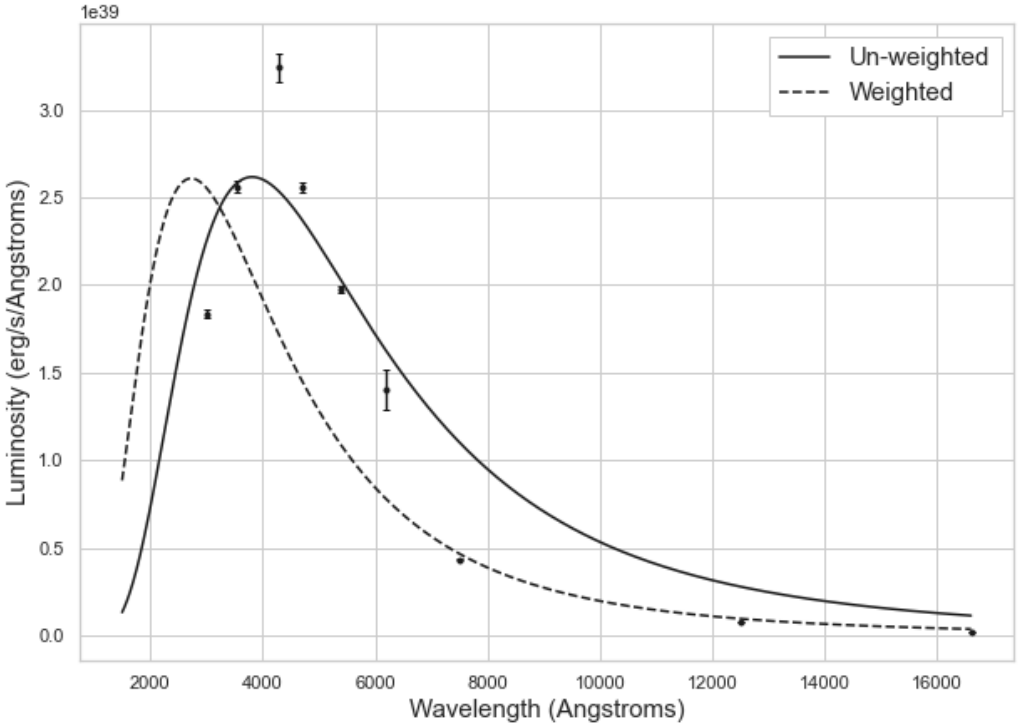

Figure 10 – Spectral energy diagram presenting luminosity data (including a UV ghost point) with error bars of 1σ*-uncertainty (circular points), against wavelength in Angstroms of SN2012fr at the epoch 1.55 after maximum B-filter brightness. Planck's blackbody function is fitted to these data points (black solid line) as a weighted fit. Some data points have error bars too small to be seen.*

From figure 10 it is clear that the quality increases with the addition of a UV ghost point as it more closely resembles a blackbody distribution and therefore the quality of its measurements and their respective uncertainties. The uncertainty in temperature is much closer to the unweighted temperature (although the weighted fit has a higher temperature – Wien's law).

The purpose for the addition of a UV ghost point is not to in anyway improve the 'fit' of Planck just for the sake of it but it is to produce expected measured results. However, this maybe a bi-product of confirmation bias. Therefore, to truly understand if SNe SED's can be approximated by Planck a larger data set maybe required to give equal weight across the full waveband, i.e., spectra.

After a number of SED's were made it became apparent that after 30 days of the SN evolution Planck no longer produced consistently sensible measurements for temperature, radius, and energy. Therefore, the conjecture is made that after 30 days the SN photosphere no longer resembled a blackbody distribution. Further evidence for this speculation can be seen in the evolution of chi-square ("goodness of fit"), temperature, energy, and radius in sections 3.2, 3.3, 3.4 & 3.5.

Epoch: +1.55 days	Radius (cm)	Temperature (K)	Chisq
Unweighted	$3.69 \pm 0.77 \times 10^{11}$	$8{,}424 \pm 865$	117
Weighted	$1.46 \pm 0.35 \times 10^{11}$	$14{,}205 \pm 2993$	40
Unweighted (ghost)	$4.47 \pm 0.76 \times 10^{11}$	$7{,}609 \pm 550$	225
Weighted (ghost)	$1.94 \pm 0.39 \times 10^{11}$	$10{,}600 \pm 1370$	84

Table 1 – Radius, temperature and chi-square values of Planck fit to SED at +1.55 days.

3.2 Chi-square evolution

The evolution of the chi-square will allow the visualisation for the 'goodness' of Planck's approximation to SED's of SN 2012fr. The chi-square will also provide further evidence for *when* in

the SN evolution Planck fits best to the SED's. A lower chi-square value corresponds to a closer fit of Planck to the SED.

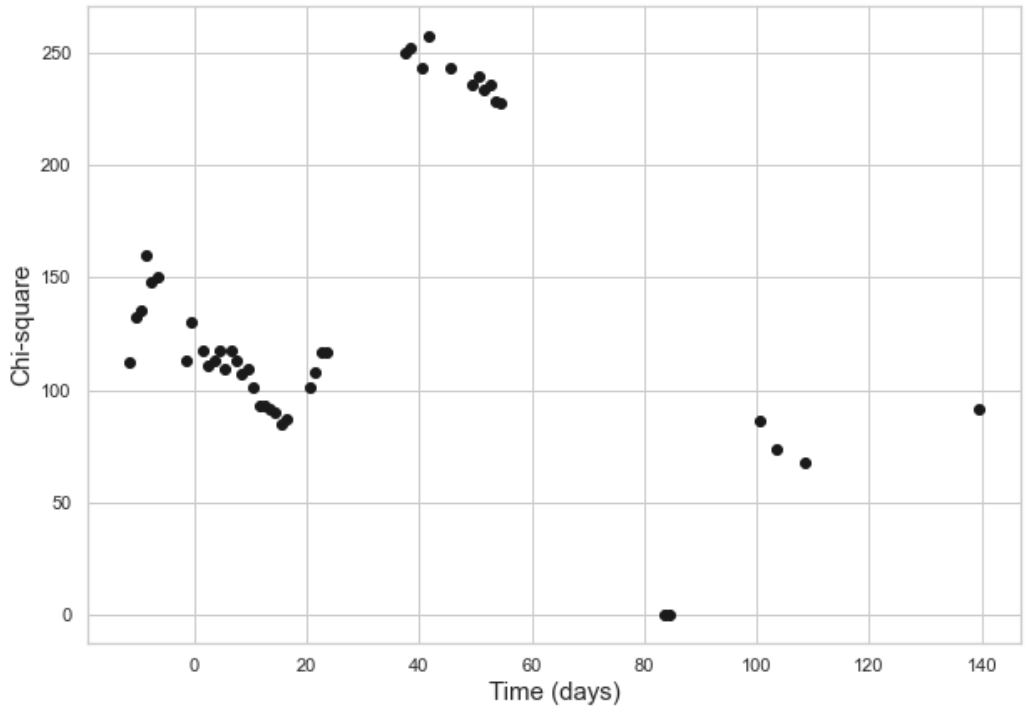

Figure 11 – Chi-square evolution of Planck's function to 45 SED's of SN 2012fr against time (days) respective to peak brightness at t = 0. Smaller chi-square represents closer fit to data.

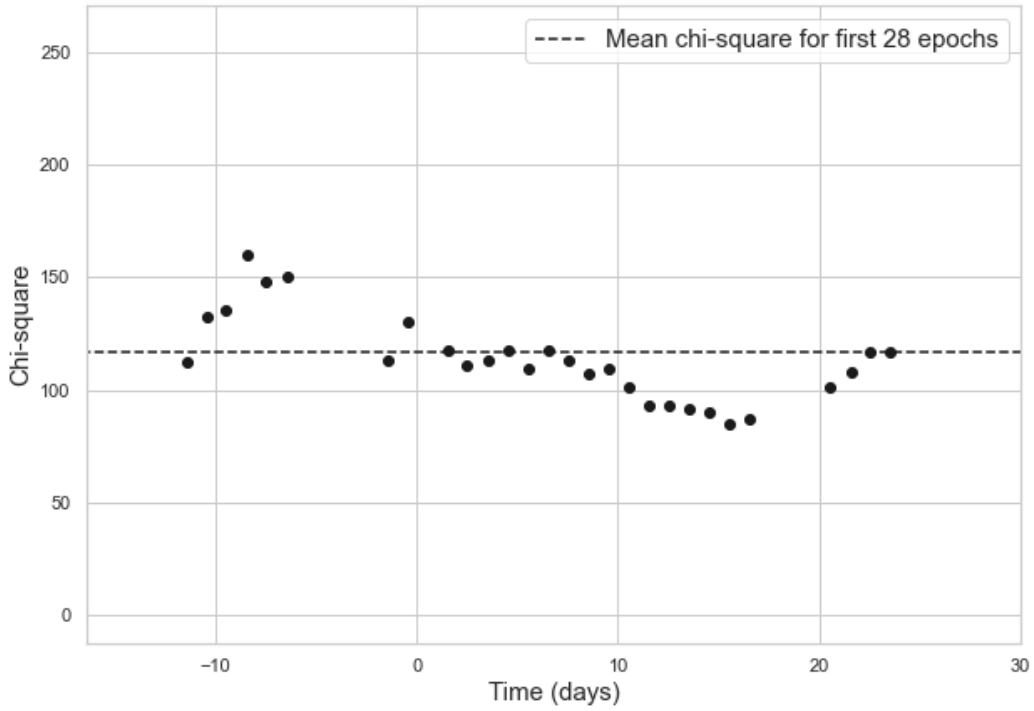

Figure 12 – Chi-square evolution of first 28 epochs plotted as SED's. Dashed line representing the mean chi-square value in that time frame. Respective to peak brightness at t = 0.

Overall, figure 11 suggests that for most of the SN evolution the photosphere emits as a blackbody. However, there are some clear differences in the quality of the fit across the evolution. It is reasnble to suggest that from -14 days to +20 days after maximum brightness that the photosphere of SN 2012fr emits as a blackbody due to the low chi-square values. However, chi-square values from around +40 to

+60 days after maximum brightness are almost double that of the earlier epochs, this would suggest that the photosphere of the SN is no longer a blackbody and Planck's function does not fit as well to the SED's. Chi-sqaure values at +80 days and beyond are found to be even lower than that of the earlier epochs however, there are not enough data points this late into the evolution to justify that Planck is a good fit to the data.

Figure 12 zooms in on the chi-square values of the first 28 epochs which show a quality fit of Planck to the SED's and remain mostly constant over this time period; a mean value of a 103. This suggests that Planck is a fair approximation to the SED's in this time period.

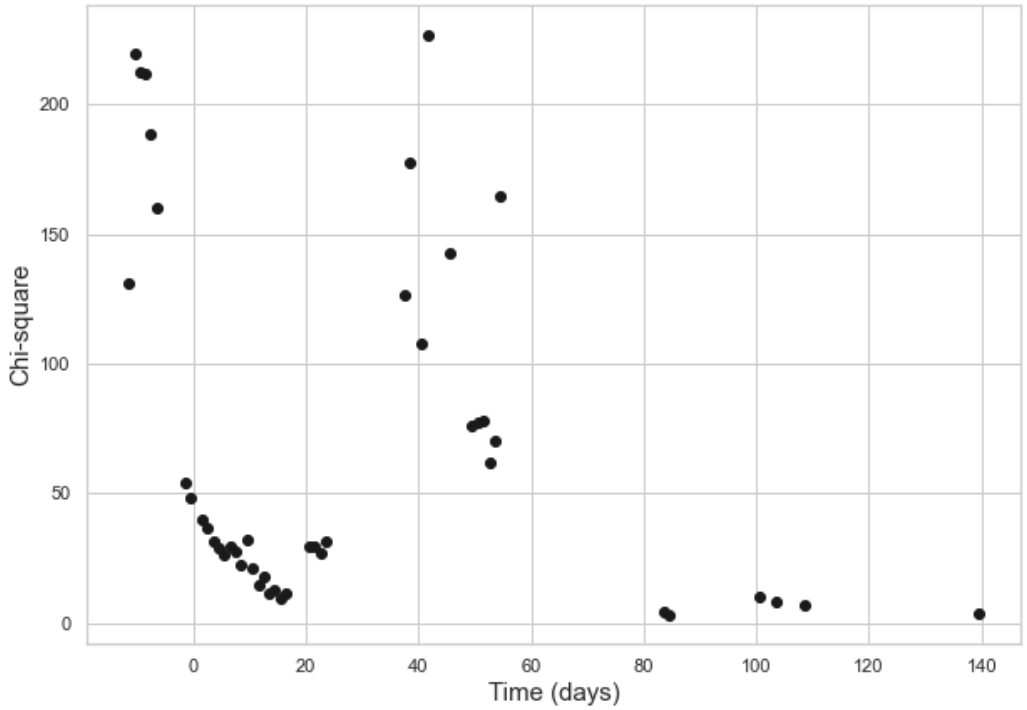

Figure 13 – Chi-square evolution of weighted fit of Planck's function to 45 SED's of SN 2012fr with time, respective to peak brightness at t = 0.

The evolution of the statisitcally weighted chi-square can be seen in figure 13. In the first ~30 days the chi-square values remain low, much alike the chi-square evolution without the addition of sigma to the fitting method (This will be called 'un-weighted' for simplicity however this does not mean it is without 'weight'). Chi-square values at around +40 to +60 days seem to increase much like the un-weighted approximation although the data points are much lower when compared with the chi-square increase in figure 11. This suggests that the addition of sigma to the fitting method for Planck produces a higher quality fit.

3.3 Temperature evolution

The evolution for the temperature of SN 2012fr can be seen in figure 14. The plot shows an initial temperature of ~8000 K and a steep increase until maximum temperature is measured as (~9500 K) at around 6 days before maximum brightness. Before maximum brightness, the opacity of the SN photosphere is completely opaque. As the photosphere expands its density decreases and the intensity of radiation emitted from the photosphere increases therefore increasing temperature until peak brightness.

$$T \propto R^{-3(\gamma-1)} \qquad \text{(Equation 14)}$$

After peak temperature there is a rapid linear decline in temperature over a time period of ~30 days; as expected (Jha et al., 2019) reaching a minimum temperature of ~5500 K. After this time period there

is a gap in the data points highlighting missing epoch measurements. Figure 14 suggests that the temperature starts to increase again at around +40 days which is unexpected as the SN would require

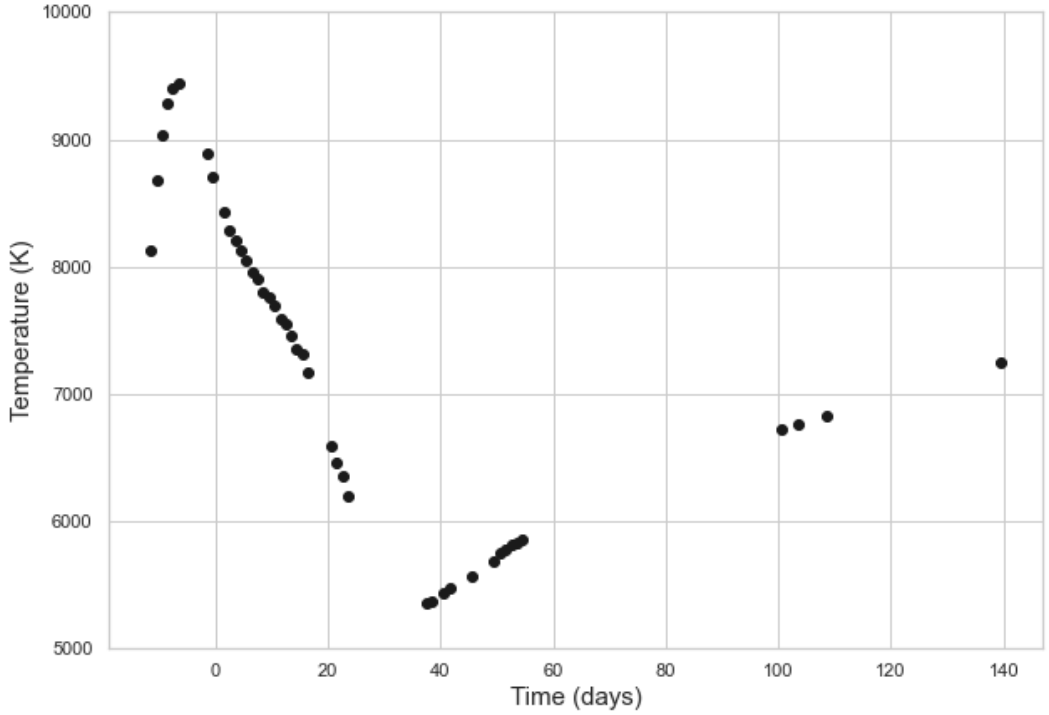

Figure 14 – Temperature (K) evolution with time (days) of SN 2012fr. Temperature measurements cover 45 epochs of SN evolution. t = 0, represents time of B – maximum brightness.

an injection of extra energy to increase the temperature again. This increase in temperature pushes the temperature measurement back up to ~7000 K. If the temperature inside the expanding photosphere of the SNe is uniform the temperature should *decrease* adiabatically with time and expansion according to equation 14 where γ is the ratio if specific heat capacities (Longair, 2011).

Therefore, the temperature evolution for SN 2012fr is expected until roughly +20 days after peak temperature where the plot no longer holds an expected result (constant temperature). This pushes for further evidence that the epochs plotted after +20 days in the time evolution of SN 2012fr cannot be fitted well to Planck's function as the measurements are no longer reasonable and are unexpected.

The decrease in quality of the fit of Planck to the data set may in fact be due to the decrease in the UV contribution to the SED with time. The decrease in the contribution from the UV could see the software give greater importance to longer wavelength data points therefore fitting a Planck function with a higher peak and so (as discussed in section 1.6) higher temperature. Evidence for this conjecture is seen in the spectra of SN 2012fr plotted by (Childress et al., 2013) seen in figure 15. It can be seen that there is an absorption feature in the IR wavelengths and a decrease in flux in the UV from 17.38 days onwards. Therefore, the SED's may still resemble a blackbody and so a fit can be approximated by Planck and so it is just the approximation of the peak that changes not the quality in the fit.

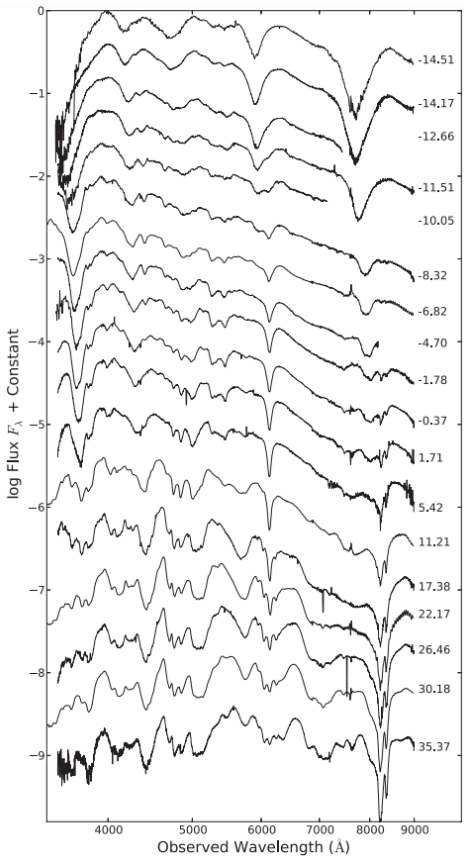

Figure 15 – Sample of SN 2012fr spectra, labelled by phase and respective to B-band maximum light (Childress et al., 2013)

3.4 Energy emission evolution

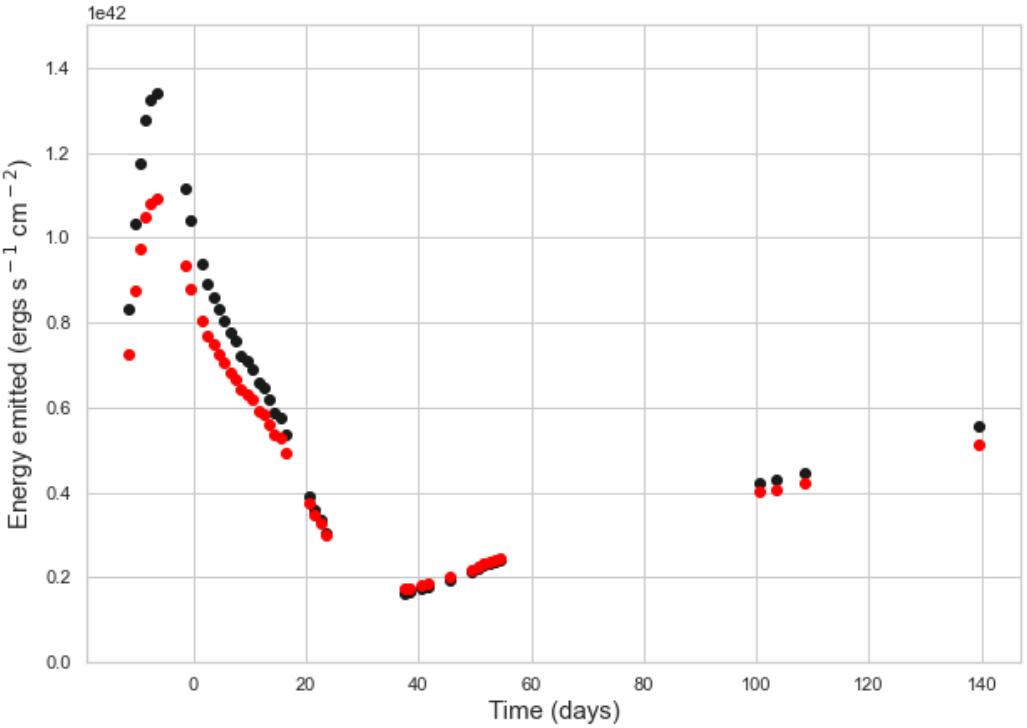

Figure 16 – Evolution of energy emitted of blackbody radiation per second per unit area of the SN photosphere with time (days) respective to peak brightness at t = 0.

Figure 16 presents the plot of energy per second per area with time. The plot shows the energy evolution for two different integration methods of the Planck function. The Trapezium method shows overall a greater energy emission than the simpsons method, however the difference between both methods is hardly significant. Both methods show the same general trend and is almost identical to the temperature evolution. The differences in the integration methods is down to the nature of the methods.

It is seen at around +40 days the energy emission starts to increase again, this maybe due to the same reason discussed in the temperature evolution: due to the smaller contribution of the UV and a higher contribution of the NIR (particularly at later epochs). As a result the software generates a Planck function with a higher peak and since energy is an integration of this function and therefore a calcuation for the area under the function, there is an overestimate for the energy emission. This again presents further evidence that Planck is not a good approximation at later epochs.

3.5 Radius evolution

The expansion of a SN photosphere is homologous where each layer expands with a velocity proportional to its radius (see equation 1). The shape of the radius evolution depends on the density profile of the SN photosphere and so the radius is measured from where $\tau = 1$. All SNe observations (seen in figure 17) show a rising/falling behaviour in the photosphere radius which is consistent with current theory (Liu et al., 2018).

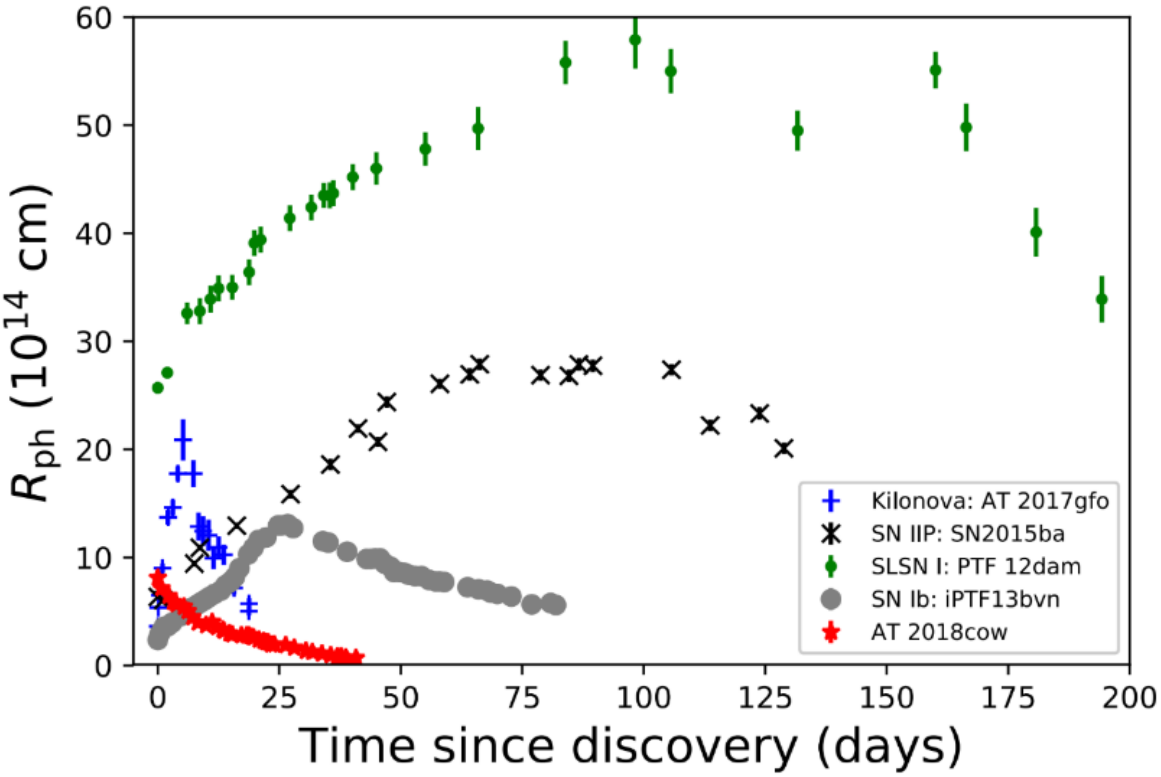

Figure 17 – Photospheric radius evolution of various optical transients (Liu et al., 2018)

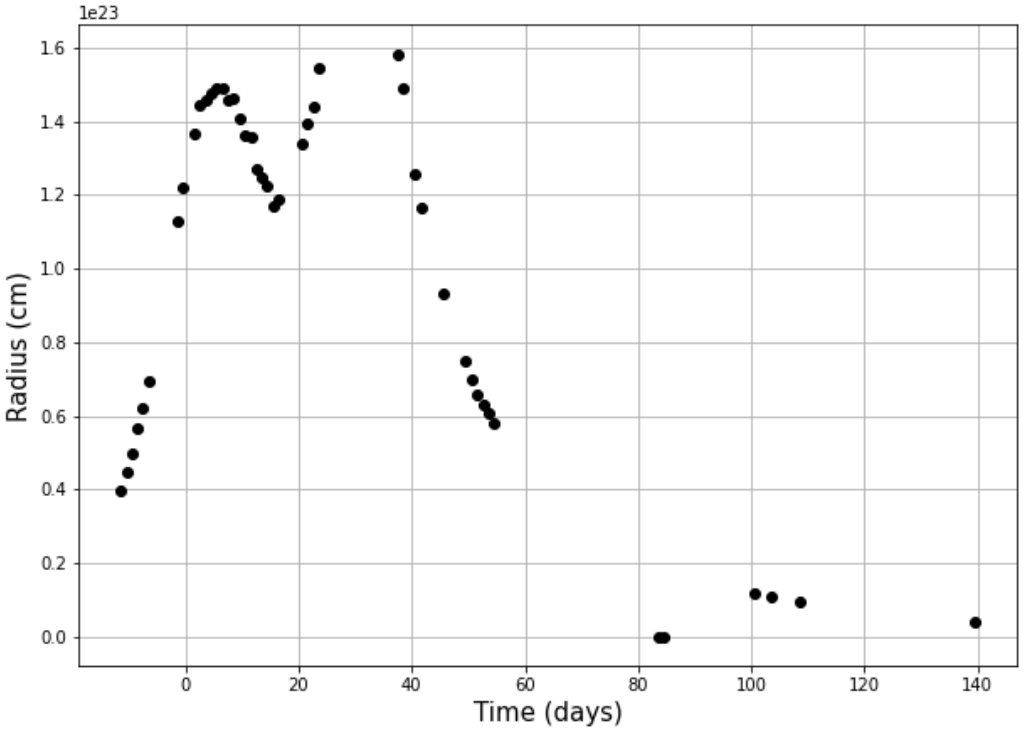

Figure 18 – Photospheric radius (cm) evolution of with time (days) of SN 2012fr. Radius measurements cover 45 epochs of SN evolution in days. respective to peak brightness at t = 0. ***Method 1***

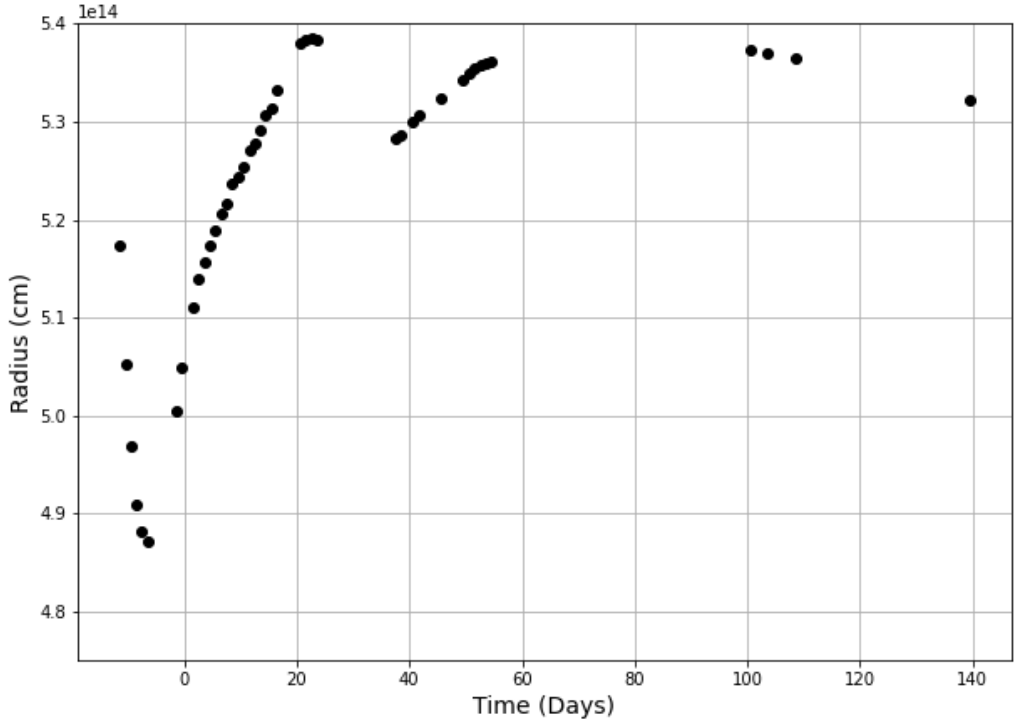

Figure 19 – Photospheric radius (cm) evolution with time (days) of SN 2012fr. Radius measurements cover 45 epochs of SN evolution. t =0, represents time of B – maximum brightness. ***Method 2***

Figure 18 presents the first plot of the SN 2012fr's photosphere radius evolution with time from measurements from the fitting method stated in section 2. The radius in figure 18 expands almost exponentially from -15 to +10 days and then decreases for the rest of the evolution. Figure 17 shows a plot from (Liu et al., 2018) where they present observations for photospheric radius evolution of many

SN types, they all show a rising and falling trend matching the behaviour of the radii in figure 18. However, between roughly +20 and +40 days the radius seems to increase and decrease dramatically. This firstly highlights a gap in the data set and secondly a possible significant change in the nature of the SN. This lapse in the expected radius evolution seen in figure 18 saw cause for comparison with the second method for producing the radius evolution.

Figure 19 presents the radius evolution of the second method. Clearly there is a significant difference. The radius begins at 5.2×10^{14} cm and decreases to 4.9×10^{14} cm and then increases again until a peak radius of 5.4×10^{14}cm where it remains roughly constant. The radius in the early part of the evolution is not expected highlighting a possible lapse in the method. Although, radius from around +20 days remains mostly constant with a small decrease of radius with time, closely resembling the radius evolution of SN Ib: iPTF13bvn seen in figure 17.

The quality of both methods remains uncertain. Both methods are based on the quality of the Planck approximation and this clearly highlights that Planck may not a solid approximation to SED's or the best method for approximating radius. Therefore, it is unclear whether the radius evolutions support the conjecture that Planck is a good approximation to SED's of SN 2012fr, but they certainly show that measurements made from the Planck fit are inconsistent are not reliable for anything conclusive on the exact evolution of the SNe radius.

3.6 Explanation for Planck's reduction in quality after +20 days of evolution

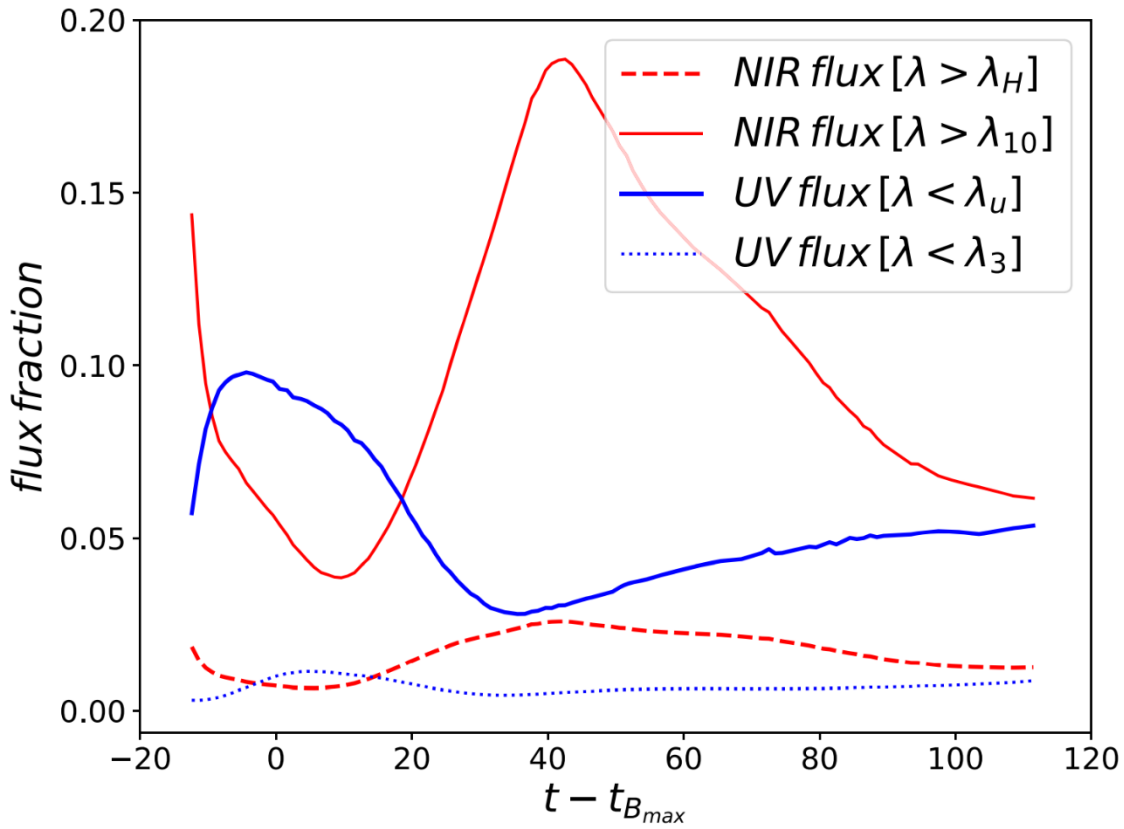

Figure 20 – Estimated ratio of UV and NIR fluxes to the total flux for SN 2012fr. The dotted and dashed lines represent the ratios for estimated fluxes beyond observed optical and NIR domain, i.e., fluxes for λ less than 3000 Å and for λ greater than the effective wavelength of the H band. For comparison purposes, the red solid line gives the flux beyond 10,000 Å and the blue solid line shows the UV flux for wavelengths less than u-band effective wavelength (Contreras et al., 2018). *Ultimately showing the UV, NIR contribution across the evolution of SN 2012fr.*

It has been stated continuously in this discussion that between +20 and +40 days after maximum brightness there is a discrepancy in the expected measurements and the quality for the fit of Planck to SED's. This is most easily visualised in the chi-square evolution (seen in figure 11) at +40 to +60 days. It has been suggested in the analysis that this may be due to the contribution of the UV or NIR causing an overestimation in temperature and therefore, energy emission. In their analysis of the bolometric light curve for SN 2012fr (Contreras et al., 2018) explain the causality for the prominent shoulder in their light curve of SN 2012fr being due to the NIR contribution rising steeply to 19% at +40 days from 4% a few days after $t_{B_{max}}$. This change in contribution seen in figure 20 explains why the chi-square values for Planck's fit increase so dramatically between +40 and +60 days and consequently why the temperature starts to increase. The temperature of SN 2012fr is not actually increasing but the NIR contribution is growing, and the UV contribution is falling pushing a for a higher peaked Planck approximation and therefore causing these unexpected measurements. The important analysis of the UV, NIR contribution made by (Contreras et al., 2018) explains why the approximation of Planck is well suited at earlier epochs, the contribution of both UV and NIR is about the same, peaking at around 10% a few days before $t_{B_{max}}$ and contribute >5% of the integrated flux only during early epochs (Contreras et al., 2018).

3.7 Discrepancy in results

It is clear from plots of measurements and chi-square evolution that after ~30 days of SN evolution there is a change in the Planck fit to the SED's and as stated this can be nicely explained by the change in contribution of the UV and NIR. However, since there are gaps in the plotted evolutions (particularly between +20 to +40 days) of temperature, radius, and energy it is difficult to tell how the evolution changes in these time periods. To remove this lapse perhaps a smaller epoch times would improve the number of epochs used in the results.

Since this research has been assessing the quality of Planck to SED's of just *one* SN it can only be concluded that only SN 2012fr does not emit as a blackbody after ~30 days of its evolution and *not all* Type Ia SNe, otherwise this is undoubtedly bias. Additionally, the epochs measured in this research only cover a total of 180 days of the SN period, which is only a fraction of the total evolution. Consequently, to make the conclusion that '*all* Type Ia SNe emit well as blackbodies at early epochs' the method seen in this research would need to be applied to a larger sample of Type Ia SNe events to make any solid conclusions about this SNe subclass.

This research does not assess the quality of the fitting method or even attempt the use of an alternative fitting method of Planck to the data. Therefore, the results of this research rely entirely on the calculations made by the 'Curve_fit' fitting method. So, to improve the quality of the method applied in this research, it may be advised to explore alternative fitting methods or to make a comprehensive assessment of the efficiency and quality of the SciPy 'Curve_fit' method.

4. Conclusion

It is found from this research that overall Planck's function is a fair approximation to SED's of SN 2012fr across the first 180-day period. In particular the first 30 days of evolution closer resemble the distribution of a blackbody spectrum than later epochs in its evolution. This is further justified by the evolution of temperature, radius, and energy, as they show expected trends during this time period. However, beyond +20 days the quality of the Planck approximation decreases highlighted the chi-square (goodness of fit) evolution. Temperature and energy begin to increase after +20 days of the SN evolution, clearly unexpected since a new injection of energy would be required. The chi-square evolution shows that the goodness of Planck's approximation to SED's halves after +20 days. This decrease in quality can be explained by the increase of the NIR and the decrease in the UV contribution (discussed in section 3.6), ensuing an increase in the height of the Planck function and so, increasing temperature (Wien's law) and energy emission measured from the approximated Planck distribution.

5. Appendix

Propagation of error for flux errors from magnitude error

$$m = -2.5log_{10}(F)$$

Apply error propagation equation and so to differentiate $log_{10}(F)$ use change of base formula:

$$log_{10}(F) = \frac{\ln(F)}{\ln(10)} \approx \frac{\ln(F)}{2.3}$$

Therefore:

$$m = -\frac{2.5}{2.3}\ln(F) + C$$

$$\frac{dm}{dF} \approx -\frac{2.5}{2.3}\frac{1}{F} = \frac{1.09}{F}$$

$$\boxed{|\sigma_m| = 1.09\frac{\sigma_F}{F}}$$

Filter	Wavelength (Å)
UV (ghost)	3000
U	3550
G	4700
R	6200
I	7500
B	4300
V	5400
J	12500
H	16600

Central Wavelengths

Filter	Flux ($10^{11} erg\ cm^{-2} s^{-1} Å^{-1}$)
UV (ghost)	850.0
U	859.5
G	466.9
R	278.0
I	185.2
B	632
V	363.1
J	31.47
H	11.38

Flux zero-points

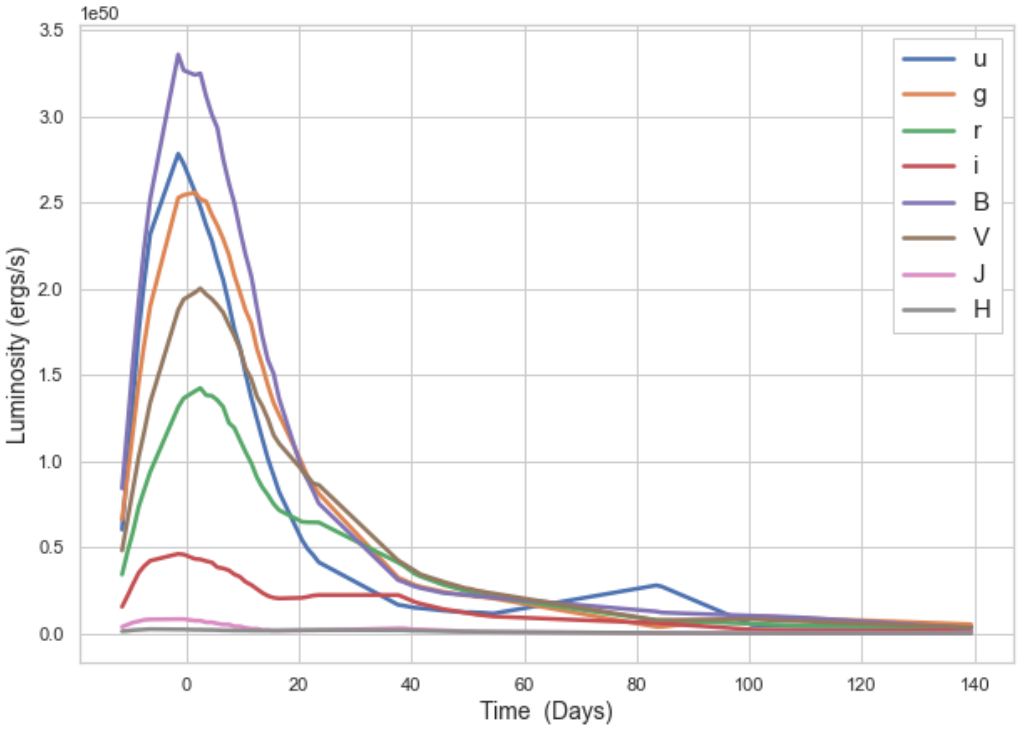

Figure 21 – Luminosty evolution

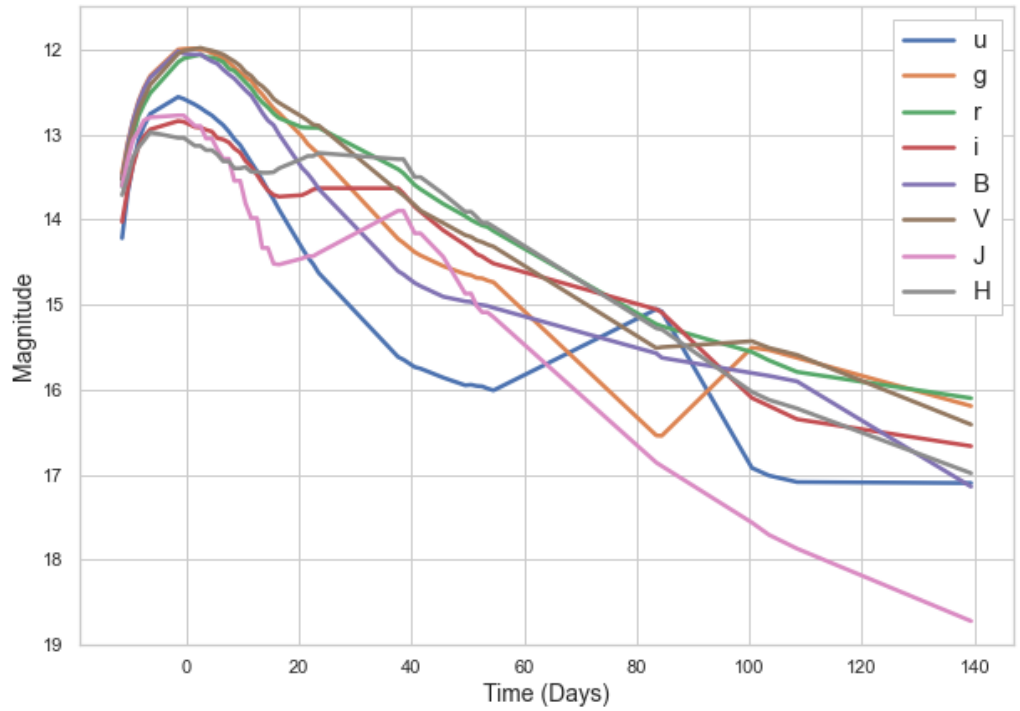

Figure 22 – Magnitude evolution

6. References

Bessell, M.S., Castelli, F., Plez, B., n.d. Model atmospheres broad-band colors, bolometric corrections and temperature calibrations for O - M stars 20.

Childress, M.J., Scalzo, R.A., Sim, S.A., Tucker, B.E., Yuan, F., Schmidt, B.P., Cenko, S.B., Silverman, J.M., Contreras, C., Hsiao, E.Y., Phillips, M., Morrell, N., Jha, S.W., McCully, C., Filippenko, A.V., Anderson, J.P., Benetti, S., Bufano, F., Jaeger, T. de, Forster, F., Gal-Yam, A., Guillou, L.L., Maguire, K., Maund, J., Mazzali, P.A., Pignata, G., Smartt, S., Spyromilio, J., Sullivan, M., Taddia, F., Valenti, S., Bayliss, D.D.R., Bessell, M., Blanc, G.A., Carson, D.J., Clubb, K.I., Burgh-Day, C. de, Desjardins, T.D., Fang, J.J., Fox, O.D., Gates, E.L., Ho, I.-T., Keller, S., Kelly, P.L., Lidman, C., Loaring, N.S., Mould, J.R., Owers, M., Ozbilgen, S., Pei, L., Pickering, T., Pracy, M.B., Rich, J.A., Schaefer, B.E., Scott, N., Stritzinger, M., Vogt, F.P.A., Zhou, G., 2013. SPECTROSCOPIC OBSERVATIONS OF SN 2012fr: A LUMINOUS, NORMAL TYPE Ia SUPERNOVA WITH EARLY HIGH-VELOCITY FEATURES AND A LATE VELOCITY PLATEAU. Astrophys. J. 770, 29. https://doi.org/10.1088/0004-637X/770/1/29

Contreras, C., Phillips, M.M., Burns, C.R., Piro, A.L., Shappee, B.J., Stritzinger, M.D., Baltay, C., Brown, P.J., Conseil, E., Klotz, A., Nugent, P.E., Turpin, D., Parker, S., Rabinowitz, D., Hsiao, E.Y., Morrell, N., Campillay, A., Castellón, S., Corco, C., González, C., Krisciunas, K., Serón, J., Tucker, B.E., Walker, E.S., Baron, E., Cain, C., Childress, M.J., Folatelli, G., Freedman, W.L., Hamuy, M., Hoeflich, P., Persson, S.E., Scalzo, R., Schmidt, B., Suntzeff, N.B., 2018. SN 2012fr: Ultraviolet, Optical, and Near-infrared Light Curves of a Type Ia Supernova Observed within a Day of Explosion*. Astrophys. J. 859, 24. https://doi.org/10.3847/1538-4357/aabaf8

Ellis, R., 2011. An Introduction to the Theory of Stellar Structure and Evolution, 2nd edn., by Dina Prialnik. Contemp. Phys. 52, 490–490. https://doi.org/10.1080/00107514.2011.580371

Flanders, T., 2006. How does the Moon's phase affect the skyglow of any given location, and how many days before or after a new Moon is a dark site not compromised? Sky Telesc. URL https://skyandtelescope.org/astronomy-resources/astronomy-questions-answers/how-does-the-moons-phase-affect-the-skyglow-of-any-given-location-and-how-many-days-before-or-after-a-new-moon-is-a-dark-site-not-compromised/ (accessed 5.10.21).

Hillebrandt, W., Kromer, M., Röpke, F.K., Ruiter, A.J., 2013. Towards an understanding of Type Ia supernovae from a synthesis of theory and observations. Front. Phys. 8, 116–143. https://doi.org/10.1007/s11467-013-0303-2

Hillebrandt, W., Niemeyer, J.C., 2000. Type Ia Supernova Explosion Models. Annu. Rev. Astron. Astrophys. 38, 191–230. https://doi.org/10.1146/annurev.astro.38.1.191

Jha, S.W., Maguire, K., Sullivan, M., 2019. Observational properties of thermonuclear supernovae. Nat. Astron. 3, 706–716. https://doi.org/10.1038/s41550-019-0858-0

Kushnir, D., Katz, B., Dong, S., Livne, E., Fernández, R., 2013. HEAD-ON COLLISIONS OF WHITE DWARFS IN TRIPLE SYSTEMS COULD EXPLAIN TYPE Ia SUPERNOVAE. Astrophys. J. 778, L37. https://doi.org/10.1088/2041-8205/778/2/L37

Liu, L.-D., Zhang, B., Wang, L.-J., Dai, Z.-G., 2018. Photospheric Radius Evolution of Homologous Explosions. Astrophys. J. 868, L24. https://doi.org/10.3847/2041-8213/aaeff6

Livio, M., Riess, A.G., 2003. Have the Elusive Progenitors of Type Ia Supernovae Been Discovered? Astrophys. J. 594, L93–L94. https://doi.org/10.1086/378765

Longair, M.S., 2011. High energy astrophysics, 3rd ed. ed. Cambridge University Press, Cambridge ; New York.

Matheson, T., Kirshner, R.P., Challis, P., Jha, S., Garnavich, P.M., Berlind, P., Calkins, M.L., Blondin, S., Balog, Z., Bragg, A.E., Caldwell, N., Concannon, K.D., Falco, E.E., Graves, G.J.M., Huchra, J.P., Kuraszkiewicz, J., Mader, J.A., Mahdavi, A., Phelps, M., Rines, K., Song, I., Wilkes, B.J., 2008. OPTICAL SPECTROSCOPY OF TYPE Ia SUPERNOVAE. Astron. J. 135, 1598–1615. https://doi.org/10.1088/0004-6256/135/4/1598

McHugh, M.L., 2013. The Chi-square test of independence. Biochem. Medica 23, 143–149. https://doi.org/10.11613/BM.2013.018

Pinto, P.A., Eastman, R.G., 2000. The Physics of Type Ia Supernova Light Curves. II. Opacity and Diffusion. Astrophys. J. 530, 757. https://doi.org/10.1086/308380

Rybicki, G.B., Lightman, A.P., 2004. Radiative processes in astrophysics, Physics textbook. Wiley, Weinheim.

Seitenzahl, I.R., Townsley, D.M., 2017. Nucleosynthesis in thermonuclear supernovae. ArXiv170400415 Astro-Ph 1955–1978. https://doi.org/10.1007/978-3-319-21846-5_87